

# Chapter 2

## Neurovascular Coupling Investigated by Simultaneous Optical Coherence Tomography and Electrophysiology

Harsha Radhakrishnan, Maria Angela Franceschini,  
and Vivek J. Srinivasan

### Abstract

A comprehensive understanding of the neurovascular coupling relationship requires the simultaneous measurement of neuronal and vascular responses and the capability to probe all layers of the cerebral cortex. Current macroscopic imaging techniques like laser Doppler imaging, diffuse optical tomography, fMRI, and PET lack spatial resolution. While two-photon microscopy is widely used in imaging the brain, it suffers from a lack of depth penetration and imaging speed. Optical coherence tomography (OCT) provides a platform for imaging the brain that potentially overcomes all of the above disadvantages, providing high-resolution cross-sectional images of light backscattered from cortical tissue. Here, we outline the experimental methods involved in simultaneous OCT (hemodynamic) and electrophysiological (neuronal) measurements to investigate neurovascular coupling in the rat somatosensory cortex. Using a spectral/Fourier domain OCT system, changes in cerebral blood flow and scattering were measured from multiple cortical layers. Simultaneous neuronal responses from layer IV using a tungsten microelectrode and surface potentials from a fire-polished ball electrode were also measured. This chapter provides details on animal preparation, instrumental setup, and data acquisition methods, and, finally, discusses potential limitations and pitfalls.

**Key words** Neurovascular coupling, Optical coherence tomography, Electrophysiology, Cerebral blood flow, anesthesia, somatosensory cortex

---

### 1 Introduction

The relationship between neuronal activity and the associated hemodynamic (blood flow, blood volume) changes is referred to as neurovascular coupling. The changes in neuronal activity due to an external stimulus are known to cause an increase in the cerebral blood flow (CBF) which supplies the activated regions of the brain with oxygenated hemoglobin [1], thereby maintaining homeostasis and normal brain function. The blood oxygen level-dependent signal obtained using functional magnetic resonance imaging (fMRI) is a measure of a deoxyhemoglobin change,

resulting from hemodynamic or metabolic changes, and may reflect underlying changes in the neuronal activity [2]. Macroscopic optical imaging techniques such as laser Doppler flowmetry [3, 4], laser speckle imaging [5], diffuse optical imaging [6, 7], and 2D intrinsic optical imaging [8, 9] have been used to investigate neurovascular coupling. Because they use diffuse light to increase the depth penetration, these methods suffer from a lack of spatial resolution. Recently, two-photon microscopy has been used for cellular and subcellular imaging of neurovascular coupling [10], but this method still does not provide enough penetration depth and imaging speed to probe the entire cortical column at once. Optical coherence tomography (OCT), analogous to ultrasound, uses the principle of low-coherence interferometry to resolve the time delay of backscattered light [11]. Recent developments in spectral/Fourier domain OCT led to dramatic increases in sensitivity and imaging speeds [12–14]. With OCT, high-resolution measurements of RBC velocities [15] are possible by measuring the Doppler shifts in the scattered light arising from moving red blood cells (RBCs). Methods such as laser Doppler and laser speckle imaging do not provide absolute measures of blood flow, especially in tissues where photon paths and optical properties are unknown. By comparison, Doppler OCT is a path length-resolved technique that yields absolute measures of blood flow by detecting Doppler-shifted backscattered light in well-defined microscopic volumes. Recently, a promising method was developed that facilitates calculations of blood flow without requiring explicit knowledge of the vessel angle [16].

In this chapter, we present methods of simultaneously measuring hemodynamic changes, using OCT, and neuronal activity, using microelectrodes and ball electrodes, in the rat somatosensory cortex. Microelectrodes are inserted into the deep cortical layers while ball electrodes are used at the cortical surface. From microelectrode recordings, we measure local field potentials (LFPs), which is a weighted sum of transmembrane currents due to synaptic and dendritic activity [17], and multi-unit activity (MUA), which is the aggregate spiking activity of a population of neurons [18]. Considering the differences in anatomy and physiology between each layer in the cortex, simultaneous measurements provide more comprehensive understanding of neurovascular coupling across all layers of the cortical column. The Materials section of this chapter outlines the OCT and electrophysiological systems. The details of the animal surgery, region of interest localization, data acquisition techniques, and an overview of the data processing algorithms are provided in the Methods section. Finally the Notes section contains some useful hints on techniques to overcome issues that can arise from this type of multimodality imaging.

## 2 Materials

A schematic of the experimental setup is shown in Fig. 1.

### 2.1 OCT System

A 1,310 nm spectra/Fourier domain OCT system was used for imaging hemodynamics in the rat cortex [19]. The system used dual superluminescent diodes (SLD) to obtain a broadband spectral output. The central wavelength was 1,310 nm and the two SLDs were combined in a 50/50 coupler to yield a bandwidth of 170 nm. Due to lower scattering at longer wavelengths, the use of an infrared wavelength light source enabled the penetration of light to deeper tissue layers in a confocal imaging geometry. The axial (depth) resolution was 4.7  $\mu\text{m}$  in air (3.5  $\mu\text{m}$  in tissue, full-width-at-half-maximum) while the transverse resolution was 7.2  $\mu\text{m}$  (full-width-at-half-maximum). A 5 $\times$  objective (Mitsutoyo) with a working distance of 3 cm was used. Using an InGaAs line scan camera (Goodrich-Sensors Unlimited, Inc.), an imaging speed of 47,000 axial scans per second was achieved. For imaging through the thinned skull, the camera sensitivity was set to “medium” to achieve a higher dynamic range.

### 2.2 Electro-physiology Setup

For measurements of deep cortical layers, a 61–70 mm long, 2–4 M $\Omega$  impedance tungsten microelectrode with a standard fine taper (FHC, ME, USA) was used. This “needle” electrode was connected to one of the channels of a 32 channel custom-built amplifier system [20].

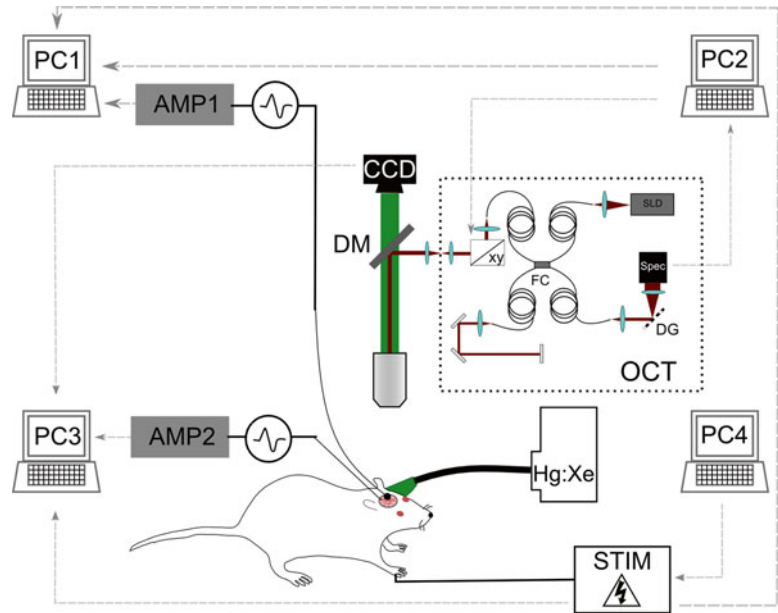


**Fig. 1** Experimental setup and data acquisition diagram for the multimodal OCT-electrophysiology experiment. Four PCs were used to monitor and relay signals

The signals from the microelectrode were then band-pass filtered between 0.1 and 500 Hz to obtain LFPs and between 500 Hz and 5 kHz to obtain MUA. This filtered data were fed through two separate PCI-bus A/D cards—a 1.25 MS/s, 12-bit card for MUA (PCI-6071E, National Instruments, USA) and a 100 kS/s, 16-bit card for LFP data (PCI-6031E, National Instruments, USA). The data were recorded using a custom software written in LabVIEW™ and stored on a computer (PC3 on Fig. 1). An Ag/AgCl electrode (4 mm diameter, Warner Instruments, USA) was used as a reference electrode and placed subcutaneously in the neck. The circuit was grounded by connecting a wire with an alligator clip on one end to the stereotactic frame.

To obtain surface potentials, a ball electrode was made by fire-polishing a silver wire (Warner Instruments, USA). The ball electrode was attached, via a crimp connector, to the electrode holder of a battery powered bioamplifier (DAM80, WPI Inc., USA). Another Ag/AgCl electrode was used as a reference for the surface potential recordings and placed adjacent to the electrode that was used as a reference for the microelectrode recordings. The signal from the electrode was band-pass filtered between 0.1 Hz and 10 kHz, recorded, and stored on a laptop (PC1 in Fig. 1). Custom software written in Matlab™ was used to acquire these signals.

### **2.3 Intrinsic Optical Imaging Setup**

Before OCT imaging and electrophysiology were performed, intrinsic optical imaging was used to determine the location of the maximal hemodynamic response. As shown in Fig. 1, a spectrally filtered Hg:Xe light source ( $570 \pm 5$  nm) illuminated the exposed cortical surface and 2-D images were obtained using a CCD camera (Infinity 2-1 M, Lumenera, CA). The CCD camera was connected by a USB cable to PC3 in Fig. 1, which acquired and saved the images. Due to the fact that oxygenated and deoxygenated hemoglobin have comparable molar extinction coefficients at 570 nm, reflectance changes around 570 nm indicated changes in blood volume. The images were later analyzed as a time series to determine the average response to a stimulus. For coarse localization of the maximal hemodynamic response, high temporal resolution was not required; hence, a lower frame rate of 1–2 Hz was used to minimize data processing time.

### **2.4 Data Acquisition Setup**

The OCT data were written to a workstation (PC2 in Fig. 1) while the microelectrode electrophysiology data and the stimulus triggers were collected on another computer (PC3 in Fig. 1). The electrical pulses for the forepaw stimulus were triggered by custom software run on a laptop (PC4 in Fig. 1), and delivered by a current stimulus isolation unit (Model A360, WPI Inc., USA). The triggers for the OCT frame acquisition, the stimulus triggers, and the responses from the surface ball electrode were acquired by yet another laptop (PC1 in Fig. 1). Although the OCT data were

acquired asynchronously, by carefully recording the locations of frames relative to the stimulus triggers, temporal information was incorporated into the linear regression procedure described below (Sect. 3.6).

---

## 3 Methods

### 3.1 Animal Surgery

The animal (rat) was initially anesthetized with isoflurane. Following this, it was placed on a homeothermic blanket (Harvard Apparatus, USA) and temperature was maintained at 37 °C. Under isoflurane, tracheostomy and cannulation of the femoral artery and vein were performed. Tracheostomy is a procedure to create an opening in the windpipe and insert a tracheal tube to control animal breathing (*see Note 1*). The arterial cannula was used to monitor blood pressure via a blood pressure transducer (SYS-BP1, WPI Inc., USA) and also perform blood glass analysis periodically to determine blood parameters such as pH, pO<sub>2</sub>, and pCO<sub>2</sub>. Cannulation of the vein was performed for administering the anesthetic during the imaging experiments. For hemodynamic measurements, it has been shown that alpha-chloralose is a suitable anesthetic [21] as it has minimal effects on respiratory and cardiovascular function [22]. Isoflurane shows minimal effects on neuronal activity but has the effect of vasodilation at higher doses [23] (*see Note 2*), while ketamine-xylazine has no impact on electrophysiology [24] and is widely used, but does impact hemodynamics [25, 26]. Anesthetics for neurovascular coupling experiments must therefore be chosen by carefully considering neuronal and vascular effects.

Following cannulation, rats were placed on a stereotaxic frame and the scalp was retracted. 2–2.5 % v/v isoflurane is administered during the craniotomy. A custom-built metal plate was then fixed on to the exposed skull using small bone screws and dental cement. A ~5 × 5 mm<sup>2</sup> area of skull over the left somatosensory cortex in the middle of the metal plate was thinned to translucency using a dental burr (*see Note 3*). A well of acrylic was built around the thinned skull area and filled with saline to keep the thinned skull region moist (*see Note 4*). Following the surgical procedure, the animal was switched from isoflurane to the anesthesia used for the experiment, e.g., alpha-chloralose. The animal should then be left to stabilize under the new anesthetic for 30 min to an hour. During this time, breathing of the animal should be monitored and blood gas analysis performed (*see Note 5*).

### 3.2 Localization of Neuronal and Vascular ROIs

Since microscopic methods are restricted to a small field of view, it is paramount that data are collected from the region of maximal neuronal and vascular responses. One way to ensure this is to localize the responses prior to collecting OCT data. For neuronal activity

localization, responses from a fire-polished ball electrode (described in Sect. 2.2) during electrical forepaw stimulation pulses (200  $\mu$ s pulses at 3 Hz for 4 s) delivered to the animal through hypodermic needles inserted in the contralateral forepaw were measured. The ball electrode was attached to the electrode holder of the stereotaxic frame and moved around to measure in a  $3 \times 3$  or  $4 \times 4$  grid within the somatosensory area where the skull has been thinned. The ball electrode was positioned in direct contact with the thinned skull surface, which was kept moist by topically adding aCSF. The goal here was to look for a response that resembles a standard mammalian-evoked potential response [27]—a large and narrow positive response component P1 followed within about 10 ms by a large and wide negative response N1 followed by two slower components P2 and N2 (*see Note 6*). For most anesthetics, a couple of measurement locations in the grid will clearly show a larger response. Once the neuronal activity has been localized, the skull at that location is further thinned and eventually removed along with the dura (*see Notes 3 and 7*) to create space for inserting the needle electrode.

After localizing the neuronal response, the animal is moved under the OCT microscope (*see Note 8*), which also has the capability to perform optical intrinsic signal imaging as shown in Figure 1. To determine the region of maximal hemodynamic response, 2-D optical imaging using a CCD camera and a 570 nm Hg:Xe light source (described in Sect. 2.3) was used. Images were acquired during a 4 min run of electrical forepaw stimulation—equal to 12 trains of 200  $\mu$ s pulses at 3 Hz for 4 s. Using custom software written in Matlab®, (Natick, MA) different regions of interest were selected. A region of decreased reflectance, resulting from increased blood volume, was then localized [28] (*see Note 9*). The region of maximal blood volume change was then used to determine the scan location for OCT imaging.

### 3.3 Setup for the Experiment

The skull should be kept moist at all times and should not be allowed to dry. For this purpose, aCSF or saline could be used. However, aCSF and saline evaporate over time, leading to a path length shift in the image that must later be corrected with post-processing. Conductive fluids that do not evaporate would thus be preferable for maintaining skull hydration. The CCD camera used to collect intrinsic images for vascular localization was used to orient the animal under the OCT objective to focus on the region of maximal blood volume change (obtained from the vascular localization). Generally speaking, the neuronal and vascular responses are well localized within a small region of approximately 1–2 mm in the somatosensory cortex for a forepaw stimulus. Thus care should be taken to ensure that the needle and the ball electrode, along with the OCT scan line, are within this small area. The working distance of the  $5\times$  objective used in this study is 3 cm. Therefore, it was imperative that extra attention be paid while

inserting the needle electrode as perpendicular as possible to the cortical surface without nicking any of the vessels. It was also important to ensure that the needle did not obstruct the OCT image. The CCD camera image and the OCT display can be used as guides to accurately insert these probes.

The needle electrode was held in place with the help of an electrode holder connected to the custom-built animal stereotactic frame. The electrode holder was tilted at a certain angle that allows for the easy insertion of the electrode (*see Note 10*). Using the CCD image as a guide, the electrode was lowered to the region where the dura has been removed and carefully inserted down to about 600–700  $\mu\text{m}$  from the brain surface until about layer IV of the cortical column. Layer IV receives the majority of the inputs to the cortex from the thalamus, which account for the positive peak P1 in the surface potential measurement. To determine if the needle is indeed in layer IV, a constant stimulus of 1 Hz was given to the animal and the responses are viewed on the screen on PC3 (in Fig. 1). It is well known that the LFP response from layer IV has an earlier response time and the largest negative amplitude than the other supragranular layers (above layer IV) [29] (*see Note 11*).

After the microelectrode was inserted, the OCT scan line position was defined. Doppler OCT images were obtained using a 5 $\times$  objective lens, which has a working distance of about 3 cm. The power in the OCT reference arm was carefully adjusted such that the spectrum was below the saturation level of the spectrometer. The OCT scan location was chosen within the region of maximal hemodynamic response (described previously) but at a place with fewer large vessels and away from the inserted microelectrode. To check if the vessels in the OCT scan line are activated, Doppler responses to electrical forepaw stimulation ( $\sim 2\text{--}3$  Hz, the maximal response for alpha-chloralose anesthesia) were verified from the on-screen display. The vessels in the imaged region should show visible velocity increases and possibly diameter changes on the on-screen display. If the vessels are inactive, the OCT scan line needs to be moved to a location with a larger hemodynamic response (*see Note 12*). At all times during the experiment, the level of the liquid covering the skull must be monitored. There should not be a decrease in the level of the liquid due to evaporation. This was important for two reasons—the skull should not be allowed to dry out and the path length for the OCT images must be maintained. Other fluids can be used instead of aCSF and saline, such as agarose or a non-volatile conductive liquid. If there is a saturating reflection from the liquid surface on the OCT image, the head of the animal can be tilted a little or the power from the reference can be reduced.

Finally, the fire-polished ball electrode was placed on the other side of the OCT scan line, away from the microelectrode. The ball electrode must be placed such that it is in contact with



the skull surface and sufficiently immersed in the liquid on the skull surface. Responses from the ball electrode must also be checked before beginning data collection (*see Note 13*).

### **3.4 Data Acquisition Procedure**

Once the animal has been placed under the microscope and the electrodes and OCT scan line are positioned, a blood gas analysis must be performed to ensure that the animal is in good physiological condition. Baseline blood flow measurements are essential to establish the physiological condition of the animal. Therefore, a Doppler OCT image consisting of 4 consecutive volumes of 256 frames with 4,096 axial scans each was acquired. It required about 25 s for each volume to be recorded. The images were acquired with the focus approximately 100  $\mu\text{m}$  below the pial surface. The CCD camera image, whose focus roughly coincided with the OCT focus, was used as a guide for the focal plane location.

Following the baseline measurement of flow, neuronal activity and OCT images were acquired during electrical forepaw stimulation. 2D OCT images  $\sim 1 \times 1 \text{ mm}^2$  were obtained by acquiring images with 4,096 axial scans at 3.3 Hz. Varying frequency stimulation between 1 and 5 Hz was applied to the forepaw of the animal. An event-related stimulus paradigm was employed [30]. A standard 6 min run consisting of 23 stimulus trains with a mean interstimulus interval of 12 s was presented with a random order of stimulus frequencies. During the 6 min run, the animal physiology (blood pressure, heart rate) was continuously monitored and any changes in the reference plane of the OCT due to evaporation of saline on the skull were noted (these can be corrected during post-processing). Upon completion of the 6 min run, additional saline was applied to the skull surface. Also, after every few of runs, it is prudent to perform blood gas analysis to ensure that the animal physiology is stable. If at any point, there is a change in blood pressure or the animal breathing is not in synchrony with the ventilator, the measurement should be stopped immediately. Generally, the rest period between runs is about 5 min. A minimum of 5–6 runs were performed per experiment. This number can be extended provided that the animal vital parameters are optimum and both the neuronal and vascular responses are robust.

### **3.5 Flow Measurement Algorithm: Absolute Baseline Blood Flow and Relative Doppler Changes**

A sample Doppler OCT image (averaged over all trials in a run) from the rat somatosensory cortex under alpha-chloralose anesthesia is shown in Fig. 2a. Large surface pial vessels and diving parenchymal vessels are marked on the image. Algorithms for determining Doppler OCT blood flow have been described previously [31]. A region of interest around a parenchymal vessel is shown in white. Figure 2b shows the blood flow responses from the marked parenchymal vessel due to stimulation. The time traces clearly show a habituation pattern with stimulus frequencies above 2 Hz.



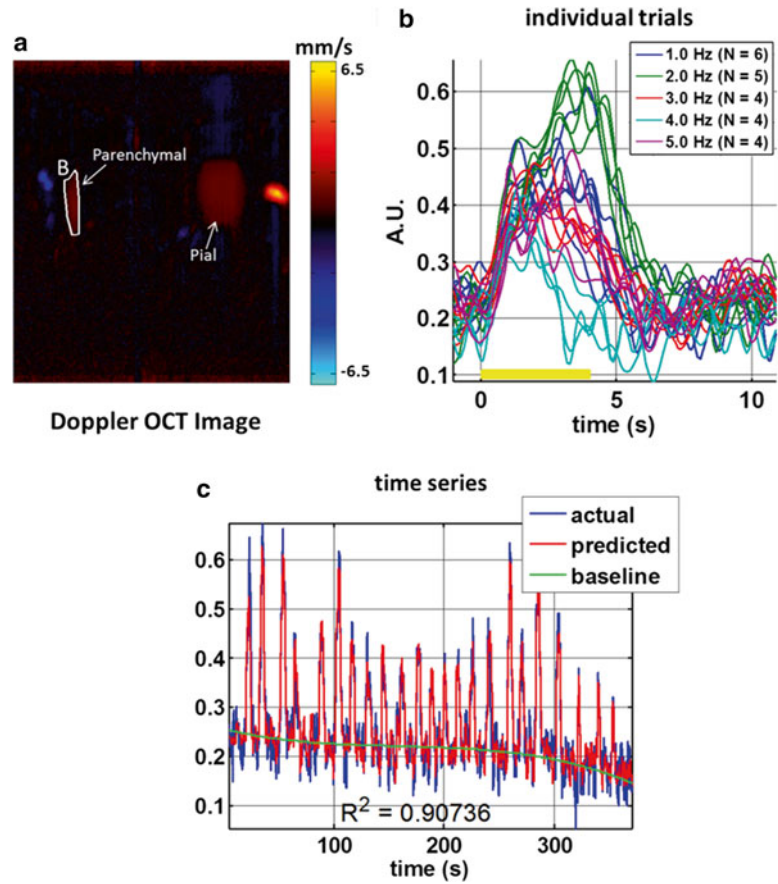


**Fig. 2** Imaging of flow responses in individual vessels using Doppler OCT. (a) Doppler OCT image with labelled parenchymal and pial vessels. A region of interest around a parenchymal vessel is shown in white. (b) Individual trials for different stimulus frequencies in the parenchymal vessel are plotted. Clearly, heterogeneous but consistent flow responses are evoked by different stimulus frequencies. (c) The flow time series (blue) along with the time series prediction based on linear regression [32] is shown. A slow polynomial term to account for baseline fluctuations was included in the regression procedure. The results of the linear regression are time courses representing responses to stimulus frequencies between 1.0 and 5.0 Hz

Figure 2c shows the flow time series in blue along with the time series prediction based on linear regression [32]. A slow polynomial term to account for baseline fluctuations was included in the regression procedure. The results of the linear regression are time courses representing responses to stimulus frequencies between 1.0 and 5.0 Hz.

An image of the OCT amplitude response to function activation is shown in Fig. 3a. This logarithmic image corresponds to the Doppler OCT image shown in Fig. 2a. The changes seen in the

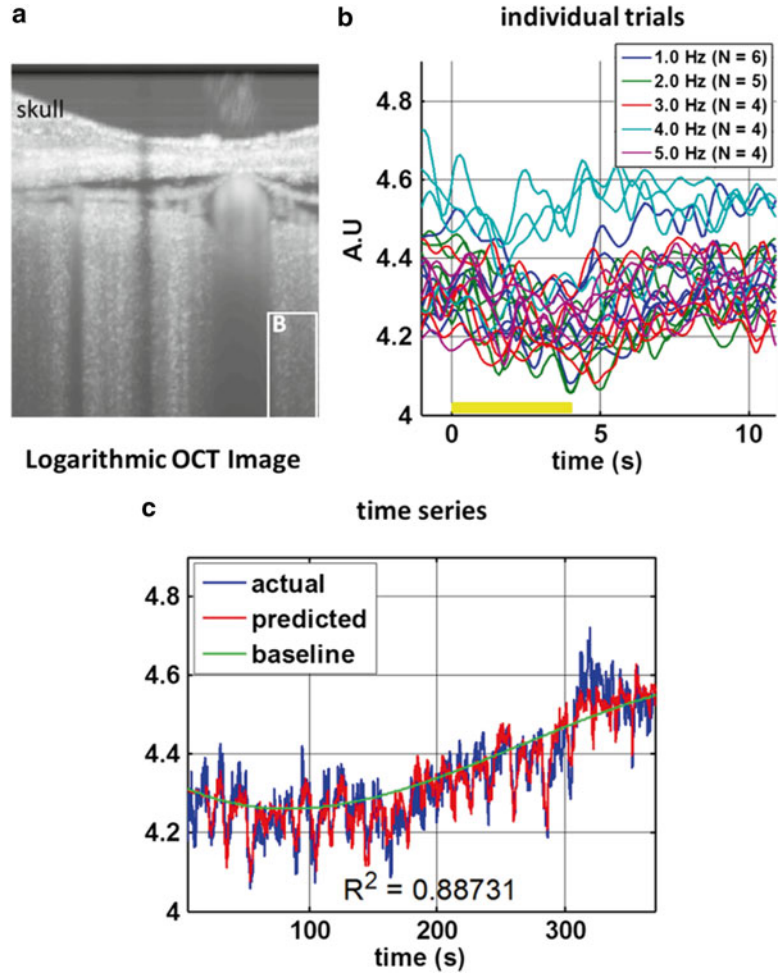


**Fig. 3** Imaging of OCT amplitude response to functional activation, most likely caused by increases in RBC density or cell swelling. (a) OCT logarithmic image corresponding to the Doppler OCT image in Fig. 2a. A region of interest is shown in white. (b) Individual trials for different stimulus frequencies, showing the integrated amplitude within the region of interest, are plotted. (c) The time series (blue) along with the time series prediction based on linear regression is shown. A slow polynomial term to account for baseline fluctuations was included in the regression procedure. The results of the linear regression are time courses representing responses to stimulus frequencies between 1.0 and 5.0 Hz

amplitude image are probably due to increases in scattering from an increase in RBC density, or cell swelling. Figure 3b shows the responses from a region of interest marked in white in Fig. 3a. The traces are integrated amplitude responses from individual trials during parametric electrical stimulation. These responses are similar to the Doppler OCT responses in Fig. 2b where changes due to

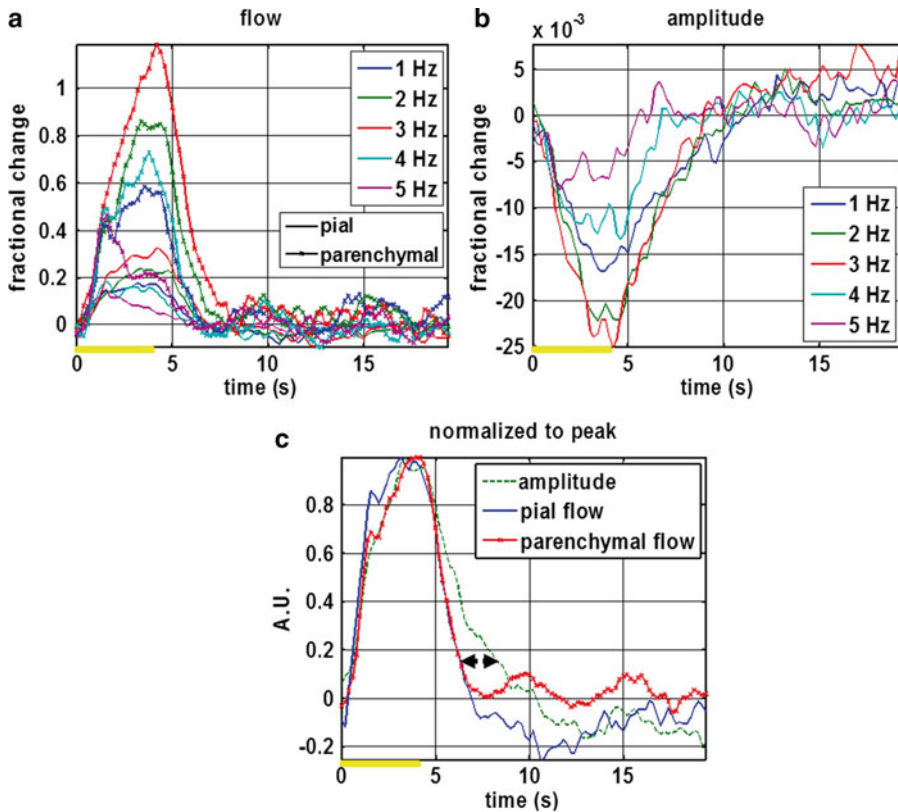


**Fig. 4** Analysis of hemodynamic responses to functional activation in a single animal, averaged across six runs. **(a)** Parenchymal fractional flow responses are much larger than pial fractional flow responses, since pial vessels are less spatially specific. However, both vessel types show similar trends as the stimulus frequency is increased. **(b)** The OCT image amplitude, from regions of interest  $>200\ \mu\text{m}$  below the surface, decreases in response to functional activation. This decrease in amplitude is likely due to an increase in scattering that accompanies an increase in red blood cell content. **(c)** Comparison of pial flow, parenchymal flow, and amplitude time courses, where all responses have been normalized to their peak. The black arrows show a delay between the flow responses and the amplitude response, which is consistent with a delayed washout of red blood cells after the stimulus ends

2–3 Hz stimulation were higher. In Fig. 3c, similar to Fig. 2c, the time series (blue) along with the time series prediction based on linear regression [32] is shown. A slow polynomial term to account for baseline fluctuations was included in the regression procedure. The results of the linear regression are time courses representing responses to stimulus frequencies between 1.0 and 5.0 Hz.

Figure 4a shows a sample group average in a different rat across 6 runs. From the figure, it is evident that the parenchymal fractional flow responses are much larger than pial fractional flow responses, since pial vessels are less spatially specific in the regions they supply or drain. Despite this difference, both vessels show a peak flow change at a 3 Hz stimulus, which is on par with changes

seen in rats under alpha-chloralose anesthesia [6]. Figure 4b shows changes in OCT image amplitude in a region of interest below about 200  $\mu\text{m}$  from the surface. The decrease in amplitude is likely due to an increase in scattering due to increased RBC content during activation [33]. Figure 4c displays a comparison between normalized pial flow, normalized parenchymal flow, and normalized relative amplitude time courses. Normalization is done with respect to the peak of the response (either positive or negative). The black dotted double headed arrow shows a delay between the flow responses and the amplitude response, which is consistent with a delayed washout of RBCs after the stimulus ends and flow has returned to baseline levels.

### 3.6 Neurovascular Coupling Analysis

To investigate neurovascular coupling, for each animal and all stimulus conditions, we assumed a linear convolution model between the measured electrical feature time series (MUA and LFP from the microelectrode and P1 and N1 surface potential components from ball electrode) and the measured hemodynamic time series from OCT. Either amplitude values, squares of peak amplitudes, or areas under the neuronal response curves can be used as inputs to the model [34]. Coefficients of determination ( $R^2$ ) between the measured and predicted flows were determined. Statistical analysis can in principle be applied to determine the significance of differences between predictions of hemodynamics by different electrophysiological measurements and components [2].

Representative data from an animal anesthetized with alpha-chloralose are shown in Fig. 5. Using the electrophysiological measures as predictors of parenchymal flow responses as described above, we found that N1 yields higher  $R^2$  values than MUA and P1. The results may be indicative of the fact that hemodynamic responses are predominantly driven by cortico-cortical transmission and not the initial thalamocortical activity in layer IV [35]. The impulse response in Fig. 4e, derived from the linear regression with N1 as a predictor of the fractional parenchymal flow response, shows a time to peak of approximately 1.2 s.

---

## 4 Notes

1. At times during the experiment, the animal may display some irregularities in breathing. One of the common problems is due to secretion into the tracheal tube, which needs to be cleaned. One way of reducing this secretion is with the injection of glycopyrrolate or atropine sulfate prior to starting the surgical procedures.
2. If isoflurane is the anesthetic used in the experiment, there is no need for femoral vein cannulation. It is advised that the artery always be cannulated to monitor blood pressure and draw

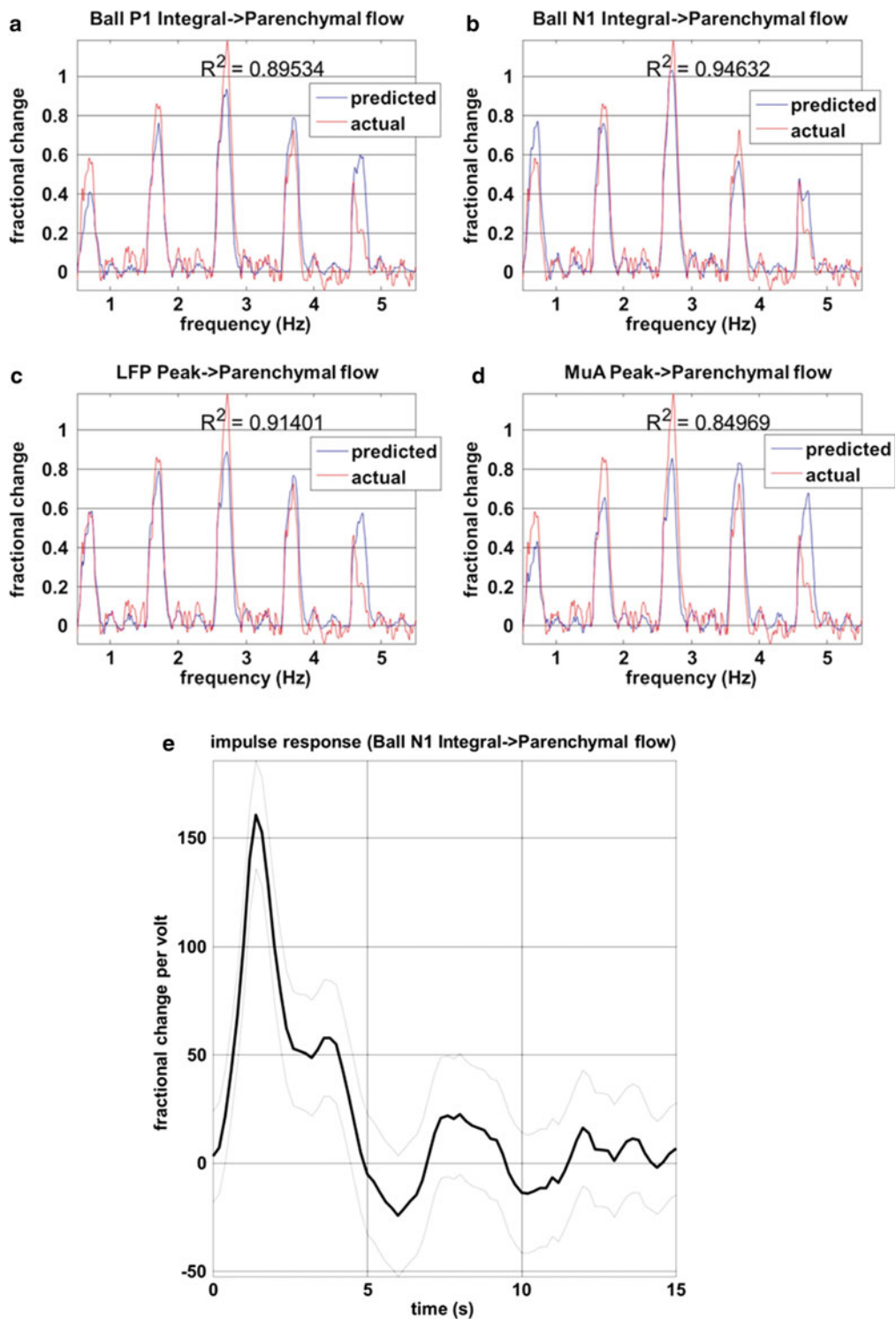


**Fig. 5** Comparison of various electrophysiological measures as predictors of fractional parenchymal flow responses across stimulus conditions (a–d). The  $R^2$  value is a measure of the goodness-of-fit. In this particular animal, anesthetized with alpha-chloralose, the integral of N1, obtained from a ball electrode on the surface of the skull, yields the highest  $R^2$  (b). (e) The impulse response, derived from the integral of N1 as a predictor of the fractional parenchymal flow responses, shows a time to peak of approximately 1.2 s. The observation that the N1 yields better predictions than P1 is consistent with the theory that cortico-cortical transmission drives the hemodynamic response

blood to perform blood gas analysis. Increase in  $p\text{CO}_2$  beyond physiological limits (40–45 mmHg) results in increased vasodilation which could hinder optimal hemodynamic responses.

3. Since the craniotomy could take up to an hour, a blood gas analysis to monitor the vital parameters should be performed during the surgery. Care should be taken to prevent drilling beyond 10  $\mu\text{m}$  to prevent injuring the brain surface or causing dural bleeding.
4. During the experiment, the liquid in the well may evaporate and change the scanning plane of the OCT imaging. Care should be taken to ensure that the scanning plane is maintained by adding additional solution between stimulus runs. Preferably, a non-evaporating conductive fluid should be used.
5. The effects of isoflurane will diminish quickly after discontinuation as it is a volatile anesthetic. But it takes time for the animal to stabilize under any new anesthetic, such as alpha-chloralose. Data collected earlier than about 45 min after switching anesthetics may not be well correlated with the rest of the experiment.
6. Neuronal localization should be performed under the same anesthetic chosen for the rest of the experiment. While measuring responses during neuronal localization, responses from the ball electrode could either be viewed on an oscilloscope or recorded on a laptop. Also, with a fire-polished ball electrode, it is possible that the two slower components may not be seen in the responses due to the impedance of the electrode (in comparison to a surface disk electrode) or due to band-pass filter settings used in the experiment (*see* Sect. 2.2). One other important aspect is to ensure that there are no stimulus-induced motion artifacts. If the stimulus current is too high, the animal may twitch visibly. One way to avoid this is to start the current at zero and slowly increase it to a point where a neuronal response is seen with imperceptible twitching of the animal.
7. The dura mater under the region where the skull is removed also has to be removed with care so as to prevent bleeding. This is done to ensure that the microelectrode can be inserted without causing any bending or breakage of the tip of the electrode.
8. Standard stereotactic frames, such as those from Kopf Instruments, are thick and bulky and therefore cannot be used to hold the animal under the OCT microscope. A custom-built animal holder was used during imaging with our OCT system.
9. In our setup, the hemodynamic localization is done after the animal is moved from the surgical table to the microscope used for OCT imaging. To perform hemodynamic localization, the

brain surface is imaged onto a CCD camera through a dichroic mirror. Also, before the hemodynamic localization, a blood gas analysis is performed to ensure that the animal physiology is stable. High  $p\text{CO}_2$  values ( $>40$  mmHg) may cause baseline vasodilation, and thus poor vascular responses during stimulation. If optimal hemodynamic responses are not observed despite robust neuronal responses, make sure that all the vital parameters and blood gases are within range for the anesthesia used. The previous Notes describe possible problems that can arise during the experiment.

10. The microelectrode has a very fine tip with the sensor at the end. It is very easy to scratch the tip on the skull surface while moving the electrode to the location where it is to be inserted into the cortex. It is very important to gently maneuver the electrode to reach the location for recording and gradually lower the micromanipulator towards the brain surface by using the CCD image on PC3 as a guide. Another important guideline is to prevent the tip from nicking any blood vessels in its path. It is advisable to find a region with low vascular density within the localized area for microelectrode insertion.
11. While inserting the microelectrode, the cortical tissue is compressed. To prevent damage, insert the microelectrode slightly beyond the required depth and then bring it back up to the required position. Doing this would release some of the pressure applied during the insertion stage. Also, insertion of the microelectrode causes a spreading depolarization. Therefore, it is advisable to wait about 15–20 min (and preferably longer) after the insertion of the electrode before collecting data. One way to confirm recovery is to assess responses to forepaw stimulation a couple of minutes after the animal exhibits stable spontaneous activity.
12. Sometimes setting up of the experiment could take a while. The animal needs to be continuously monitored during this period. If there is no visible vessel dilation due to the stimulation, a blood gas analysis should be performed, and ventilation parameters should be changed accordingly. All the vital parameters should also be checked to ensure that they are within physiological ranges.
13. During the initial testing for responses from the various imaging modalities, it should be ensured that there is no coordinated increase in the animal blood pressure due to the stimulus. If this does occur, one possible cause may be insufficient anesthesia, which can be rectified by increasing the dose of the maintaining anesthetic. Another possible cause could be that the stimulus intensity is too high. Reducing the current should help prevent stimulus-induced blood pressure increases.



## Acknowledgement

This research is supported by the US National Institutes of Health (NIH) grants R01-EB001954 and R00-NS067050.

## References

1. Roy S, Sherrington S (1890) On the regulation of the blood-supply of the brain. *J Physiol* 11: 85–108
2. Logothetis NK et al (2001) Neurophysiological investigation of the basis of the fMRI signal. *Nature* 412:150–157
3. Fabricius M, Lauritzen M (1996) Laser-Doppler evaluation of rat brain microcirculation: comparison with the [ $^{14}\text{C}$ ]-iodoantipyrine method suggests discordance during cerebral blood flow increases. *J Cereb Blood Flow Metab* 16:156–161
4. Dirnagl U et al (1989) Continuous measurement of cerebral cortical blood flow by laser-Doppler flowmetry in a rat stroke model. *J Cereb Blood Flow Metab* 9:589–596
5. Boas DA, Dunn AK (2010) Laser speckle contrast imaging in biomedical optics. *J Biomed Opt* 15:011109
6. Franceschini MA et al (2010) The effect of different anesthetics on neurovascular coupling. *Neuroimage* 51:1367–1377
7. Culver JP et al (2003) Diffuse optical tomography of cerebral blood flow, oxygenation, and metabolism in rat during focal ischemia. *J Cereb Blood Flow Metab* 23:911–924
8. Martin C et al (2013) Complex spatiotemporal haemodynamic response following sensory stimulation in the awake rat. *Neuroimage* 66: 1–8
9. Malonek D, Grinvald A (1996) Interactions between electrical activity and cortical microcirculation revealed by imaging spectroscopy: implications for functional brain mapping. *Science* 272:551–554
10. Shih AY et al (2012) Two-photon microscopy as a tool to study blood flow and neurovascular coupling in the rodent brain. *J Cereb Blood Flow Metab* 32:1277–1309
11. Huang D et al (1991) Optical coherence tomography. *Science* 254:1178–1181
12. Leitgeb R, Hitzengerger CK, Fercher AF (2003) Performance of Fourier domain vs. time domain optical coherence tomography. *Opt Express* 11:889–894
13. de Boer JF et al (2003) Improved signal-to-noise ratio in spectral-domain compared with time-domain optical coherence tomography. *Opt Lett* 28:2067–2069
14. Choma MA et al (2003) Sensitivity advantage of swept source and Fourier domain optical coherence tomography. *Opt Express* 11: 2183–2189
15. Chen Z et al (1997) Optical Doppler tomographic imaging of fluid flow velocity in highly scattering media. *Opt Lett* 22:64–66
16. Srinivasan VJ et al (2010) Quantitative cerebral blood flow with optical coherence tomography. *Opt Express* 18:2477–2494
17. Eccles JC (1951) Interpretation of action potentials evoked in the cerebral cortex. *Electroencephalogr Clin Neurophysiol* 3: 449–464
18. Mitzdorf U (1987) Properties of the evoked potential generators: current source-density analysis of visually evoked potentials in the cat cortex. *Int J Neurosci* 33:33–59
19. Srinivasan VJ et al (2010) Rapid volumetric angiography of cortical microvasculature with optical coherence tomography. *Opt Lett* 35: 43–45
20. Ulbert I et al (2001) Multiple microelectrode-recording system for human intracortical applications. *J Neurosci Methods* 106: 69–79
21. Austin VC et al (2005) Confounding effects of anesthesia on functional activation in rodent brain: a study of halothane and alpha-chloralose anesthesia. *Neuroimage* 24:92–100
22. Nakao Y et al (2001) Effects of anesthesia on functional activation of cerebral blood flow and metabolism. *Proc Natl Acad Sci U S A* 98: 7593–7598
23. Eger EI II (1984) The pharmacology of isoflurane. *Br J Anaesth* 56:71S–99S
24. Kochs E, Bischoff P (1994) Ketamine and evoked potentials. *Anaesthesist* 43:S8–S14
25. Crosby G, Crane AM, Sokoloff L (1982) Local changes in cerebral glucose utilization during ketamine anesthesia. *Anesthesiology* 56: 437–443
26. Lei H et al (2001) The effects of ketamine-xylazine anesthesia on cerebral blood flow and oxygenation observed using nuclear magnetic

- resonance perfusion imaging and electron paramagnetic resonance oximetry. *Brain Res* 913:174–179
27. Di S, Barth DS (1991) Topographic analysis of field potentials in rat vibrissa/barrel cortex. *Brain Res* 546:106–112
  28. Frostig RD et al (1990) Cortical functional architecture and local coupling between neuronal-activity and the microcirculation revealed by in vivo high-resolution optical imaging of intrinsic signals. *Proc Natl Acad Sci U S A* 87:6082–6086
  29. Radhakrishnan H, Wu W, Franceschini MA (2011) Study of neurovascular coupling by modulating neuronal activity with GABA. *Brain Res* 1372:1–12
  30. Dale AM (1999) Optimal experimental design for event related fMRI. *Hum Brain Mapp* 8: 109–114
  31. Srinivasan VJ, Chan AC, Lam EY (2012) Doppler OCT and OCT angiography for in vivo imaging of vascular physiology. In: Liu G (ed) *Selected topics in optical coherence tomography*. InTech, Rijeka
  32. Frykholm P et al (2005) Relationship between cerebral blood flow and oxygen metabolism, and extracellular glucose and lactate concentrations during middle cerebral artery occlusion and reperfusion: a microdialysis and positron emission tomography study in nonhuman primates. *J Neurosurg* 102:1076–1084
  33. Srinivasan VJ et al (2009) Depth-resolved microscopy of cortical hemodynamics with optical coherence tomography. *Opt Lett* 34: 3086–3088
  34. Franceschini MA et al (2008) Coupling between somatosensory evoked potentials and hemodynamic response in the rat. *Neuroimage* 41:189–2003
  35. Iadecola C (2004) Neurovascular regulation in the normal brain and in Alzheimer's disease. *Nat Rev Neurosci* 5:347–360

Neurovascular Coupling Methods

Schwartz, T.; Ma, H.; Schwartz, T.H. (Eds.)

2014, XIX, 332 p. 120 illus., 99 illus. in color., Hardcover

ISBN: 978-1-4939-0723-6

A product of Humana Press